Contribution from Ames Laboratory-DOE[1] and the Department of Chemistry, Iowa State University, Ames, Iowa 50011

Chemistry of Polar Intermetallic Compounds. Study of Two Zr_5Sb_3 Phases, Hosts for a Diverse Interstitial Chemistry

Eduardo Garcia and John D. Corbett*

Received February 3, 1988

A variety of synthesis routes, some phase properties, and two single-crystal X-ray studies have established something of the nature of the Zr–Sb system in the neighborhood of 65 atom % zirconium. Samples prepared by vapor-phase transport or by annealing either elemental powders or arc-melted products at 1000–1100 °C yield the Mn_5Si_3 form of Zr_5Sb_{3+x}. This is a true binary phase that is nonstoichiometric over the range of $0.0_0 \leq x \leq 0.4_2$. Study of a single crystal with $x = 0.16$ (1) from an arc-melted sample has established that the extra antimony in this structure is bonded in an interstitial site in the center of a chain of confacial zirconium octahedra (space group $P6_3/mcm$, $Z = 2$, $a = 8.4267$ (5) Å, $c = 5.7856$ (6) Å, $R = 2.7\%$, $R_w = 3.4\%$). Many other atoms may also be bound at this site. Binary Zr–Sb samples in the range $0 \leq x \leq \sim 0.2$ melt incongruently to form the foregoing phase plus a second, new, high-temperature, stoichiometric form of Zr_5Sb_3 in the Y_5Bi_3 structure (space group *Pnma*, $Z = 4$, $a = 7.465$ (1) Å, $b = 8.801$ (1) Å, $c = 10.865$ (2) Å, $R = 2.8\%$, $R_w = 2.9\%$). The two structure types are further described and compared.

Introduction

The large family of metal-rich binary compounds that are formed between a particular transition metal (T) and the diverse main-group (M) nonmetals, metalloids, and adjacent metals exhibit a remarkable range of stoichiometries, structures, and properties. Nonetheless, this group of compounds also possesses some common characteristics regarding electronic and bonding features, namely those that arise because of sizable differences in valence-state ionization energies of component atoms. As a result, we can expect that the main-group element in all of these will contribute heavily to the lower lying (and therefore filled) valence bands, particularly when bonded to an earlier transition metal element, while a strong heteroatom T–M bonding will contribute greatly to the stability of the phases. Although it would be simplistic and wrong to identify all of these as "salts", their polar nature does make the foregoing electronic relationship very probable.

Phases that are rich in the transition-metal component will also exhibit T–T bonding. Valence electrons that remain after filling the predominately main group element (M) states will usually be in conduction states or bands that are largely associated with the electropositive metal (T) component. These electrons can be described as delocalized in T–T bonds, clusters, or extended arrays, and the compounds are characteristically diamagnetic or Pauli paramagnetic rather than paramagnetic because of the absence of localized, unpaired spins on the T atoms. Just how far to the left in the periodic table the main-group element can lie and still have the compound exhibit no or a minimal overlap between its filled, principally M valence band and the T-based conduction band remains to be determined. However, we can anticipate that many of the main-group metals or metalloids will participate in what we here term "polar intermetallics", compounds in which strong heteroatomic bonding and the above valence generalities apply.

Of course, transition-metal-poor phases in the same systems may often exhibit significant bonding between the main-group elements, and these interactions may make an appreciable if not a dominant contribution to the conduction band. For example, we have found that many of the zirconium antimonide phases appear to fall into one or other of the limiting types just described. Some aspects of the M-rich type of behavior were noted in a recent consideration of the $ZrSb_2$ phases,[2] and considerably more regarding particular examples of T-rich phases will become apparent through forthcoming reports on the chemistry of Zr_5Sb_3 as well as of Zr_5Sn_3, La_5Ge_3, Ca_5Sb_3, and analogous systems.[3]

Our attention was first drawn to the zirconium–antimony system by early reports[4,5] of an unusual ability of the phase Zr_5Sb_3 (as well as a host of other compounds in the Mn_5Si_3-type structure) to bond one of several third elements Z in a particular interstitial position to form an isostructural Zr_5Sb_3Z phase. Indeed, we have found that the range of Z elements that can so participate is remarkable.[3] Our early efforts on this Zr_5Sb_3Z chemistry naturally also focused on the character of the host material Zr_5Sb_3 and on the general nature of the phase relationships in the Zr–Sb system in the neighborhood of 65 atom % zirconium. The detailed results of this investigation were beyond the scope of our previous report that considered all of the compounds formed in this binary system,[2] and so they are presented here.

The first report of a binary Zr–Sb phase[6] and the first structure type identified[7,8] were for Zr_5Sb_3, and as such one might suppose it would be the best characterized compound of the system. But at the start of this work it was not clear whether Zr_5Sb_3 is a true binary compound or an impurity-stabilized ternary phase. The latter idea was first advanced because the volume per atom was about 4.5% greater than the value interpolated between other binary Zr–Sb phases as then assigned[9] and, later on, because of an apparent tendency of a number of phases with the Mn_5Si_3 structure to take up impurities.[4,5] Our investigation of these points reveals that the situation is not quite so simple since there are in fact two Zr_5Sb_3 phases. One does indeed have the Mn_5Si_3 structure, but this is better formulated as Zr_5Sb_{3+x}, $0 \leq x \leq 0.4$. The second structure occurs for a stoichiometric Zr_5Sb_3 phase that crystallizes in the Y_5Bi_3 arrangement.

Experimental Procedures

Materials. The zirconium metal used in all experiments was reactor-grade, crystal bar material that had been cold-rolled and then cut into pieces ca. 0.5 × 10 × 10 mm. Powdered zirconium was obtained through decomposition of ZrH_2. The nominal dihydride was made by reaction of Zr pieces with H_2 at 750 °C and the product ground into a powder, passed through a 150-mm sieve, and then heated slowly to 700 °C under vacuum (10^{-5} Torr) in a molybdenum boat until no further H_2 was evolved. The lattice parameters of the metal powder thus obtained were within experimental error of literature values.[10] The reagent-grade antimony (Allied Chemical and Dye Co.) did not produce any dross upon fusion, which means nonmetal contamination was at a low level, and its SEM-EDX analysis showed no detectable impurities. The material was

(1) Ames Laboratory is operated for the U.S. Department of Energy by Iowa State University under Contract No. W-7405-Eng-82. This research was supported by the Office of Basic Energy Sciences, Materials Sciences Division.

(2) Garcia, E.; Corbett, J. D. *J. Solid State Chem.* **1988**, *74*, 440, 452.
(3) Garcia, E.; Hurng, W.-M.; Kwon, Y.-U.; Guloy, A.; Corbett, J. D., to be submitted for publication.
(4) Nowotny, H.; Benesovsky, F. In *Phase Stability in Metals and Alloys*; Rudman, P. S., Stringer, J., Jaffee, R. I., Eds.; McGraw-Hill: New York, 1966; p 319.
(5) Pearson, W. B. *The Crystal Chemistry and Physics of Metals and Alloys*; Wiley-Interscience: New York, 1972; p 718.
(6) Russi, R. F.; Wilhelm, H. A. Publication AECD-3610, U.S. Atomic Energy Commission, 1951.
(7) Boller, H.; Parthé, E. *Monatsh. Chem.* **1962**, *94*, 225.
(8) Schubert, K.; Meissner, H. G.; Pötzschke, M.; Rossteutscher, W.; Stolz, E. *Naturwissenschaften* **1962**, *49*, 57.
(9) Rossteutscher, W.; Schubert, K. *Z. Metallkd.* **1965**, *56*, 813.
(10) Holmberg, B.; Dagerham, T. *Acta Chem. Scand.* **1961**, *15*, 919.

0020-1669/88/1327-2353$01.50/0

Table I. Crystallographic Data for Refined Structures

compd	Zr_5Sb_3 (Y_5Bi_3)	$Zr_5Sb_{3.16}$ (Mn_5Si_3)
space group	*Pnma*	$P6_3/mcm$
Z	4	2
lattice params[a]		
a, Å	7.465 (1)	8.4267 (5)
b, Å	8.801 (1)	
c, Å	10.865 (2)	5.7856 (6)
V, Å^3	713.9 (2)	355.79 (6)
cryst size, mm	0.22	0.25
	0.07	0.04
	0.05	0.04
2θ(max), deg; octants	55; $\pm h,k,l$	55; $\pm h,\pm k,l$
no. of reflns		
checked	1892	2057
obsd[b]	1179	1312
indep	657	144
abs coeff, μ, cm^{-1} (Mo Kα)	180	181
transmissn coeff range	0.336–0.404	0.340–0.463
R(av)	0.022	0.047
secondary extinctn coeff (10^{-4})	0.018	0.030
R[c]	0.028	0.027
R_w[d]	0.029	0.034
no. of variables	50	17

[a] From refined Guinier powder data. [b] $F_o > 3\sigma_F$ and $I_o > 3\sigma_I$. [c] $R = \sum||F_o| - |F_c||/\sum|F_o|$. [d] $R_w = [\sum w(|F_o| - |F_c|)^2/\sum w|F_o|^2]^{1/2}$, $w = 1/\sigma_F^2$.

powdered by grinding. All powdered starting materials were handled only in the drybox. All products could be briefly handled in air, but they were usually stored under inert conditions as they are generally not stable in air overnight and impurity effects were a particular concern of these investigations.

Syntheses. Some of the samples studied were prepared on a 1-g scale by arc melting pieces of the elements on a water-cooled copper hearth in a Centorr 55A single-arc furnace. This was filled with argon at slightly greater than atmospheric pressure, and the atmosphere in the furnace was first gettered by melting zirconium before proceeding to the reaction mixture. Antimony was added in a slight (~10%) excess in order to compensate for losses through vaporization that occurred for the most part in the initial 2–3 s. The final composition was determined by weight loss with the assumption that this arose solely from antimony volatilization. The correctness of this procedure has been confirmed[2] by the ability to obtain single-phase samples of known compositions in this way, which for the usual Guinier powder X-ray diffraction sensitivity means that any impurity phase must be present at less than 2–4 mol %. The equilibrium vapor pressure of antimony above the molten Zr–Sb alloys is low enough that the solidified button can be turned over and remelted repeatedly with only slight further weight changes. Some of the arc-melted buttons were subsequently annealed in open Ta crucibles that had been sealed within fused-silica jackets under an atmosphere of Ar.

Some compositions were prepared by the reaction of the mixed powders at elevated temperatures (~1100 °C). Stoichiometric amounts of the elements were first ground together with an agate mortar and pestle in the drybox and were then pressed into a pellet at 8 kbar. This mixture was allowed to react in a Ta crucible again sealed within a fused-silica jacket under Ar. The temperature of the reaction was first maintained at 550 °C overnight so that the elements would react sufficiently to avoid subsequent antimony fusion. Any prior melting of this within the pellet would be deleterious in reducing the diffusion interface between the compacted grains.

An additional synthetic technique utilized was vapor-phase transport starting with powders of the elements in stoichiometric proportions. These were contained in weld-sealed Ta tubes that were themselves sealed inside an evacuated silica jacket to prevent oxidation. Iodine used as the transporting agent was added in the form of ZrI_4.

X-ray Diffraction. Powder patterns of samples mounted between pieces of cellophane tape were obtained by utilizing an Enraf-Nonius Guinier camera, Cu Kα_1 radiation (λ = 1.54056 Å), and NBS silicon as an internal standard. The known 2θ values of the standard's lines were fitted to a quadratic in their position on the film and lattice constants of the sample then calculated by a least-squares fit to 18–35 indexed 2θ values. This procedure regularly produces lattice constants with standard deviations of a few parts in 10^4. The identification of structure type by powder pattern means was accomplished through comparison of line positions and intensities in an experimental pattern with the distributions calculated for known structure types by the program POWD 5.[11]

Table II. Synthesis Conditions for Zr_5Sb_3 Preparative Reactions

reacn	compositions (Zr:Sb)	annealing conditions[a] temp, °C	time, days	products[b]
1	$Zr_{0.68}Sb_{0.32}$ (2.13)			Zr_3Sb, Zr_5Sb_3-Y
2	$Zr_{0.66}Sb_{0.34}$ (1.94)	1200	0.6	X,[c] Zr_5Sb_3-Y
3	$Zr_{0.65}Sb_{0.35}$ (1.86)	950	2	Zr_2Sb, Zr_5Sb_3-M
4	$Zr_{0.626}Sb_{0.374}$ (1.67)			Zr_5Sb_3-Y, Zr_5Sb_3-M
5	$Zr_{0.60}Sb_{0.40}$ (1.50)	1100	4	
		750	1	Zr_5Sb_3-M
6	$Zr_{0.56}Sb_{0.44}$ (1.27)	900	5	Zr_5Sb_3-M, $ZrSb_{1-x}$

[a] Following arc melting. [b] Types of structures: Y = Y_5Bi_3; M = Mn_5Bi_3. [c] Unknown phase with an approximate Zr_2Sb composition that is stable in the temperature range ~1000–1400 °C.[2]

Single-crystal investigations of samples sealed in glass capillaries were carried out at room temperature with the aid of a four-circle Syntex $P2_1$ diffractometer equipped with a monochromator and Mo Kα radiation. Programs for data averaging, absorption correction (ϕ scan, tuned every 10°), Fourier synthesis, and least-squares refinement and the sources of scattering factors (including anomalous dispersion corrections) have been referenced previously.[12] Experimental details of the single-crystal X-ray diffraction data collection and handling are reported in Table I.

The first study listed in the table required that the possible Y_5Bi_3[13] and Yb_5Sb_3[14] types be distinguished. Both occur in the space group *Pnma*, but with the a and c axes interchanged. Data were initially collected in the Yb_5Sb_3-type setting, for which the a axis is longer, but after the data were averaged, the systematic extinctions were found to place it in the nonstandard setting *Pcmn*. The a and c axes were then interchanged, and the h and l parameters adjusted accordingly to put the data in the standard orientation *Pnma* for the Y_5Bi_3 type. The structure refinement initiated with the aid of positional parameters from Y_5Bi_3 proceeded smoothly. In the final three cycles all variables except the multiplicity of Zr(1) were simultaneously refined to yield R = 2.8% and R_w = 2.9%.

A single crystal of the Mn_5Si_3 form of Zr_5Sb_3 was obtained from an as-cast preparation of overall composition $Zr_5Sb_{3.0}$ in which the powder pattern showed a mixture of this with the second Zr_5Sb_3 phase (above). The diffractometer data exhibited systematic absences consistent with the space group of the Mn_5Si_3 structure, $P6_3/mcm$. The least-squares refinement was carried out with the initial positional parameters of Mn_5Si_3.[5] The refinement proceeded in a well-behaved manner, and after several cycles the convergence of the variable positional parameters, anisotropic thermal parameters, and secondary extinction correction factor yielded an R value of 0.071. At this point a Fourier map revealed an electron density peak at the origin of the unit cell of approximately 7 e/Å^3. This was assumed to represent partial occupancy of the interstitial site by antimony and was refined as such. The distance of the surrounding Zr atoms to this site is 2.53 Å, which excludes the possibility of its occupancy by an oxygen or similar-sized atom. The final agreement factors converged at R = 0.027 and R_w = 0.034 with refinement of occupancies as well except for that of Zr(1). The formula so determined was, by atom type, $Zr_2Zr_{3.00(2)}Sb_{3.01(2)}Sb_{0.161(7)}$, which compares with coefficients of 2, 3, 3, and 1, respectively, for full occupancy of each site.

Results and Discussion

Examples of specific synthesis conditions utilized are listed in Table II, and lattice parameters for the relevant products are given in Table III.

When samples of composition Zr_5Sb_3 are prepared by arc melting, the powder patterns of as-cast samples are always those of a two-phase mixture. One phase could be identified as Zr_5Sb_3 with the Mn_5Si_3 structure (Zr_5Sb_3-M), but it exhibited lattice parameters significantly larger than those obtained after annealing either the stoichiometric material or samples in which this form of Zr_5Sb_3 was in equilibrium with Zr_2Sb, the next zirconium-richer

(11) Clark, C. M.; Smith, D. K.; Johnson, G. J. *A FORTRAN IV Program for Calculating X-Ray Diffraction Patterns-Version V*; Department of Geosciences, The Pennsylvania State University: University Park, PA, 1973.
(12) Hwu, S.-J.; Corbett, J. D.; Poeppelmeier, K. R. *J. Solid State Chem.* **1985**, *57*, 43.
(13) Wang, Y.; Gabe, E. J.; Calvert, L. D.; Taylor, J. B. *Acta Crystallogr., Sect. B: Struct. Crystallogr. Cryst. Chem.* **1976**, *B32*, 1440.
(14) Brunton, G. D.; Steinfink, H. *Inorg. Chem.* **1971**, *10*, 2301.

Table III. Structure Types and Lattice Parameters for Zr_5Sb_3 Products[a]

reacn	product	structure type	lattice params, Å
2	Zr_5Sb_3-Y	Y_5Bi_3	a = 7.465 (1) b = 8.801 (1) c = 10.865 (2)
3	Zr_5Sb_3-M	Mn_5Si_3	a = 8.4175 (6) c = 5.7678 (6)
4[b]	$Zr_{6.5}Sb_3$-Y	Y_5Bi_3	a = 7.467 (1) b = 8.797 (1) c = 10.872 (2)
4[b]	Zr_5Sb_3-M	Mn_5Si_3	a = 8.468 (1) c = 5.800 (1)
5	Zr_5Sb_3-M	Mn_5Si_3	a = 8.518 (1) c = 5.844 (1)
6	Zr_5Sb_3-M	Mn_5Si_3	a = 8.573 (1) c = 5.872 (1)
1[b]	Zr_5Sb_3-Y	Y_5Bi_3	a = 7.468 (1) b = 8.787 (3) c = 10.865 (3)

[a] Data for other products listed in Table II are given in ref 2. [b] Unannealed samples.

phase[2] (4 vs 3, Tables II and III). The second product of the arc-melting reaction was subsequently identified as Zr_5Sb_3 in the Y_5Bi_3 structure (Zr_5Sb_3-Y). The latter phase was also observed in a ~50:50 mixture with Zr_3Sb in an as-cast sample with an overall composition of $Zr_{2.1}Sb$. A single crystal of the then-unknown phase (from reaction 1) was indexed on the diffractometer, which then allowed refined lattice parameters to be obtained from the Guinier powder data (Table III). This unit cell information together with the intensity distribution enabled the structure of the unknown phase to be identified as that of either the Y_5Bi_3[13] or the Yb_5Sb_3[14] type. These two structures are very similar and cannot be easily distinguished by powder diffraction alone.

Zr_5Sb_3-Y. A single-crystal structural investigation was carried out in order to determine which structural modification was actually adopted, because it was initially thought that this phase was an antimony-deficient Zr_5Sb_{3-x} phase in view of the circumstances (above) under which it was first observed. However, simultaneous refinement of site occupancies for all but one atom yielded a formula unit of $Zr_{4.99(1)}Sb_{3.02(3)}$, indicating that the compound is effectively stoichiometric. The possibility that the Y_5Bi_3-type structure of Zr_5Sb_3-Y contained and was stabilized by a third impurity atom was eliminated by the final Fourier map, which contained no residual electron density peaks greater than 0.5 e/Å^3. Such a ternary behavior for this structure type has been observed in other systems, however.[3]

The refined variables and resulting interatomic distances for Zr_5Sb_3-Y are listed in Table IV. A projection of the structure onto (010) is shown in Figure 1, in which shadings of the atoms represent the fractional y coordinates (i.e., an atom at $y = {}^1/_4$ is one-fourth shaded). Although the Zr(3) and Sb(1) atoms lie near $y = {}^1/_2$ and 0, respectively, and are shown half-filled, they are not fixed at these positions and are actually displaced from these values by 0.48 and 0.07 Å, respectively. It is subtle differences in these displacement features that distinguish the Y_5Bi_3 and Yb_5Sb_3 structures.

The zirconium atoms at $y = {}^3/_4$ in Figure 1 have been connected so as to aid the visualization of the structure, but these lines do not represent the shorter separations or actual bonds. This zirconium net of triangles and distorted hexagons is repeated, slightly displaced, by zirconium atoms at $y = {}^1/_4$ to generate a network of interconnected triangular and hexagonal prisms aligned along $\bar{b}$. The Sb(2) atoms at $y = {}^1/_4$ and ${}^3/_4$ are slightly displaced from the centers of the opposite faces of the hexagons toward opposite edges. All the zirconium trigonal prisms are centered by Sb(1) atoms at $y \simeq {}^1/_2$, and each prism shares vertical edges to form the side faces of three hexagonal prisms. The latter are seen to be centered on the side faces of the cell as depicted in Figure 1.

Table IV. Refined Positional Parameters and Interatomic Distances in Zr_5Sb_3-Y (Y_5Bi_3 Type)

Positional Parameters

atom	site	x	y	z
Sb(1)	8(d)	0.0709 (1)	−0.0078 (1)	0.1756 (1)
Sb(2)	4(c)	0.0779 (1)	${}^1/_4$	0.4566 (1)
Zr(1)	4(c)	0.4699 (2)	${}^1/_4$	0.4898 (1)
Zr(2)	4(c)	0.3075 (2)	${}^1/_4$	0.2249 (1)
Zr(3)	8(d)	0.1998 (1)	0.5543 (1)	0.4425 (1)
Zr(4)	4(c)	0.1475 (2)	${}^1/_4$	0.7130 (1)

Interatomic Distances (Å)[a]

Sb(1)–Zr(2)	2.927 (1)	Zr(2)–Zr(1)	3.125 (2)
Sb(1)–Zr(4)	2.945 (1)	Zr(2)–2Sb(1)	3.193 (1)
Sb(1)–Zr(1)	2.951 (1)	Zr(2)–Zr(1)	3.437 (2)
Sb(1)–Zr(1)	2.992 (1)	Zr(2)–2Zr(3)	3.519 (2)
Sb(1)–Zr(4)	3.023 (1)	Zr(2)–2Zr(3)	3.663 (1)
Sb(1)–Zr(3)	3.083 (1)	Zr(2)–2Zr(2)	3.777 (1)
Sb(1)–Zr(3)	3.085 (1)	Zr(3)–Sb(2)	2.833 (1)
Sb(1)–Zr(3)	3.106 (1)	Zr(3)–Sb(2)	2.912 (1)
Sb(1)–Zr(2)	3.193 (1)	Zr(3)–Sb(1)	3.083 (2)
Sb(1)–Sb(2)	3.806 (1)	Zr(3)–Sb(1)	3.085 (1)
Sb(1)–Sb(1)	3.963 (1)	Zr(3)–Zr(1)	3.099 (2)
Sb(2)–Zr(2)	2.824 (2)	Zr(3)–Sb(1)	3.106 (1)
Sb(2)–2Zr(3)	2.833 (1)	Zr(3)–Zr(4)	3.239 (2)
Sb(2)–Zr(4)	2.835 (2)	Zr(3)–Zr(3)	3.375 (2)
Sb(2)–2Zr(3)	2.912 (1)	Zr(3)–Zr(1)	3.393 (1)
Sb(2)–Zr(1)	2.951 (2)	Zr(3)–Zr(3)	3.445 (2)
Sb(2)–Zr(2)	3.048 (2)	Zr(3)–Zr(2)	3.519 (2)
Sb(2)–2Zr(1)	3.806 (1)	Zr(3)–Zr(4)	3.544 (2)
Zr(1)–2Sb(1)	2.951 (1)	Zr(3)–Zr(2)	3.663 (1)
Zr(1)–Sb(2)	2.951 (2)	Zr(3)–Zr(4)	3.996 (1)
Zr(1)–2Sb(1)	2.992 (1)	Zr(4)–Sb(2)	2.835 (2)
Zr(1)–2Zr(3)	3.099 (2)	Zr(4)–2Sb(1)	2.945 (1)
Zr(1)–Zr(2)	3.125 (2)	Zr(4)–2Sb(1)	3.023 (1)
Zr(1)–2Zr(3)	3.393 (1)	Zr(4)–Zr(3)	3.239 (2)
Zr(1)–Zr(4)	3.419 (2)	Zr(4)–Zr(1)	3.419 (2)
Zr(1)–Zr(2)	3.437 (2)	Zr(4)–Zr(1)	3.491 (2)
Zr(1)–Zr(4)	3.491 (2)	Zr(4)–2Zr(3)	3.544 (2)
Zr(2)–Sb(2)	2.824 (2)	Zr(4)–2Zr(4)	3.822 (1)
Zr(2)–2Sb(1)	2.927 (1)	Zr(4)–2Zr(3)	3.996 (1)
Zr(2)–Sb(2)	3.048 (2)		

[a] Distances less than 4.0 Å.

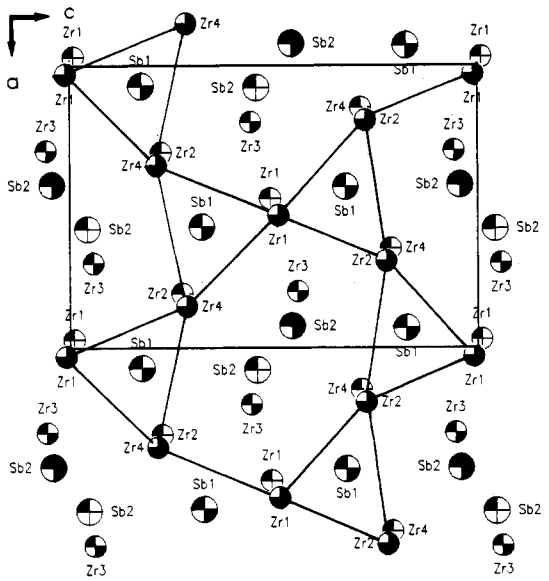

Figure 1. Projection of the Zr_5Sb_3 (Y_5Bi_3 type) structure onto (010). The shading of each atom reflects its y coordinate. The ellipsoid sizes are arbitrary. The triangular-hexagonal net of zirconium atoms at $y = {}^3/_4$ is emphasized.

The hexagonal prisms contain pairs of Zr(3) atoms at $y \simeq {}^1/_2$ that may also be viewed as capping the three rectangular faces of the trigonal prisms. Finally, the above network of prisms that lie between $y = {}^1/_2$ and $y = {}^3/_4$ naturally also share opposite faces

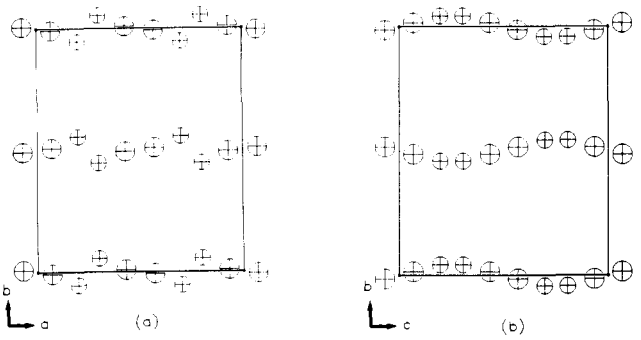

Figure 2. Projection of (a) the Y_5Bi_3-type (Zr_5Sb_3) and (b) the Yb_5Sb_3-type structures onto (001) and (100), respectively. Smaller circles are the rare-earth-metal atoms. In the interest of clarity, only the atoms around these planes are drawn. The difference between the structure types can be seen in the buckled layers at $y = 0, {}^1/_2$.

to form an infinite array along $\vec{b}$.

The atom nets around $y = {}^1/_4, {}^3/_4$ shown for this example of the Y_5Bi_3-type structure are almost identical with those in the closely related Yb_5Sb_3 type, but the layers at $y = 0, {}^1/_2$ are buckled differently. The difference is shown in Figure 2, where only the positions of atoms that lie near the (020) planes are projected, Sb(1) and Zr(3) in the Y_5Bi_3-type structure in Figure 2a and the equivalent atoms in the Yb_5Sb_3 type in Figure 2b. Differences resulting from these slight perturbations are not easily distinguished in a powder pattern. The reason for the difference in the two structures is not easy to perceive.

The single-crystal refinement of Zr_5Sb_3-Y confirmed the 5:3 stoichiometry within experimental error, and the effective invariance of lattice constants determined from powder diffraction data for Zr_5Sb_3-Y in equilibrium with either Zr_3Sb or Zr_5Sb_3-M (reactions 1 and 4, Table II) indicates that the composition does not vary significantly from this ratio. Likewise, as-cast and annealed samples appeared to be the same.

There is a definite temperature dependence, however, for the formation of Zr_5Sb_3-Y, since this has only been observed in samples prepared by arc melting. When stoichiometric amounts of zirconium and antimony powders are sintered ($T \leq 1100$ °C), only Zr_5Sb_3-M is formed. The Zr_5Sb_3-Y phase is therefore presumed to be a high-temperature modification, but the transformation temperature is not known. Annealing as-cast products has yielded inconsistent results. As an extreme example, a sample of $Zr_5Sb_{3.0}$ composition obtained by arc melting and annealed at 1100 °C for 1 week showed no apparent change in the proportions of Zr_5Sb_3-Y and Zr_5Sb_3-M, but an arc-melted sample of composition $Zr_5Sb_{2.7}$ (Zr/Sb = 1.86) with Zr_5Sb_3-Y (and Zr_3Sb) present that was annealed at 950 °C for 2 days yielded only Zr_5Sb_3-M along with Zr_2Sb. (Zr_2Sb is unstable at high temperatures.[2]) The transformation is apparently sluggish and must depend on unidentified variables. The reverse reaction, Zr_5Sb_3-M to Zr_5Sb_3-Y, must take place above 1100 °C.

Zr_5Sb_3-M. Synthesis. The Mn_5Si_3-type Zr_5Sb_3 can be synthesized by vapor-phase transport, arc melting, or sintering powders. The vapor-transport reactions are difficult experiments because of the high temperature required to deposit Zr_5Sb_3 from gaseous iodide species. Hot-wire reactions were only partially successful. These were carried out by sealing stoichiometric amounts of the powdered elements and a small quantity (~25 mg) of SbI_3 in a Pyrex tube that also contained a Ta wire with external connections through which a current could be passed. The entire apparatus was placed in a furnace at 300 °C and the wire heated to ~1300 °C. This produced Zr_5Sb_3-M, but unfortunately, the composition of the material deposited on the hot wire was very dependent on temperature. As product formed, the resistance and hence the temperature of the wire dropped, and $ZrSb_{1-x}$ or even ZrSb[2] might eventually be formed. The deposited Zr_5Sb_3-M was presumably not of uniform composition either.

Iodide-transport reactions at 1300 °C were also investigated under nominally isothermal conditions. Stoichiometric amounts of the components and a small quantity of SbI_3 (~5 mg) were sealed in tantalum containers and these heated within an evacuated mullite tube. Unfortunately, the vacuum ($\sim 10^{-5}$ Torr) was not adequate to maintain compositional integrity during the 2-week reaction period. About 10% ZrO_2 was always formed, and no single crystals of the Zr_5Sb_3-M product were obtained that were suitable for X-ray studies.

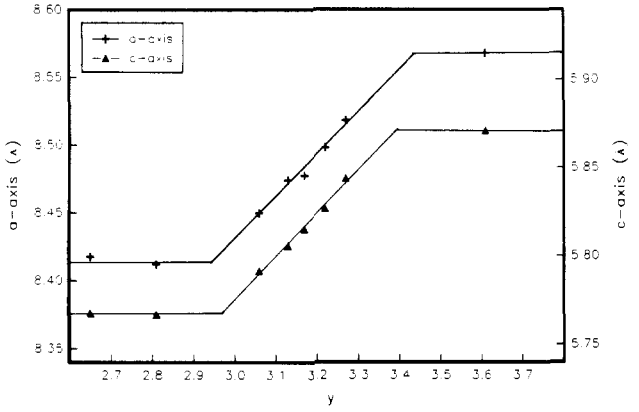

Figure 3. Lattice parameter vs composition plot for Zr_5Sb_y ($y = 3 + x$). Additional data points in the two-phase regions that lie outside the compositional range shown were also used in fixing the horizontal lines.

Synthesis by arc melting was generally satisfactory for compositions between about $Zr_5Sb_{3.2}$ and $Zr_5Sb_{3.4}$, with sharp diffraction lines being obtained for both as-cast and annealed (1000–1100 °C, 3 days) products. Arc-melted samples more antimony-rich than $Zr_5Sb_{3.4}$ were biphasic and consisted of $Zr_5Sb_{\sim 3.4}$-M and $ZrSb_{1-x}$ (FeSi type).[2] When the overall composition was closer to Zr_5Sb_3, Zr_5Sb_3-Y was also found in as-cast samples, and annealing such multiphase products yielded inconsistent results (above). On the other hand, Zr_5Sb_3-Y was never seen when Zr_5Sb_3 was prepared by sintering ($T \leq 1100$ °C) or vapor transport.

It was difficult to achieve equilibrium via powder reactions at 1000–1100 °C. The samples had to be reground and repelleted two or three times and maintained at temperature for a total of 1–2 weeks. Temperatures nearer 1300 °C would probably be more suitable, but equipment with that capability was not available to us at that time. Most samples were, therefore, prepared by arc melting followed by annealing of these more intimate mixtures, for which 3 days at 1000 °C was found to be sufficient.

The fact that Zr_5Sb_3-M is a true binary compound and not an impurity-stabilized phase[9] was established by its reproducible and quantitative yield in many different reactions and via several different synthetic techniques. These investigations led to the determination that Zr_5Sb_3-M does exhibit a substantial homogeneity range, however. Lattice dimension data were obtained from products of arc-melted and annealed systems in which the final compositions Zr_5Sb_y were assigned by attributing all weight loss on melting to antimony volatilization. Lattice constant evidence for the homogeneity range is shown graphically in Figure 3. Data for the central, single-phase region can be seen to intersect those independently established[2] for the antimony-poor and antimony-rich limits in two-phase systems at Zr_5Sb_y compositions of about $y = 2.97$ and 3.4_2. It is possible that the slightly substoichiometric lower limit is not real but an artifact reflecting a small systematic error. This consideration presumably applies to the other phase limit as well. Linear least-squares fits of the uncorrected lattice parameters shown yield the equations

$$a = 0.31455y + 7.4864 \text{ Å}$$

$$c = 0.24465y + 5.04131 \text{ Å}$$

with correlation factors of 0.9998 for each.

The high-antimony limit for this phase does not appear to be particularly temperature-dependent, judging from lattice constants obtained for this phase from as-cast vs those for annealed samples. Lattice constant data also indicate that almost the entire composition range can be obtained by vapor-phase transport, though

Table V. Refined Parameters and Interatomic Distances for $Zr_5Sb_{3.16}$-M (Mn_5Si_3 Type)

Positional Parameters					
atom	site	refined occupancy	x	y	z
Sb(1)	6(g)	1.003 (7)	0.6083 (1)	0	$^1/_4$
Zr(1)	4(d)	1	$^1/_3$	$^2/_3$	0
Zr(2)	6(g)	1.000 (7)	0.2466 (3)	0	$^1/_4$
Sb(2)	2(b)	0.081 (4)	0	0	0

Interatomic Distances, Å			
Sb(1)–2Zr(2)	2.890 (1)	Zr(2)–2Sb(2)	2.532 (2)
Sb(1)–4Zr(1)	2.974 (1)	Zr(2)–2Sb(1)	2.890 (1)
Sb(1)–Zr(2)	3.048 (2)	Zr(2)–Sb(1)	3.048 (2)
Sb(1)–2Zr(2)	3.141 (1)	Zr(2)–2Sb(1)	3.141 (1)
Sb(1)–2Sb(1)	3.421 (1)	Zr(2)–4Zr(1)	3.545 (1)
Zr(1)–2Zr(1)	2.893 (1)	Zr(2)–4Zr(2)	3.562 (1)
Zr(1)–6Sb(1)	2.974 (1)	Zr(2)–2Zr(2)	3.599 (4)
Zr(1)–6Zr(2)	3.545 (1)		

not without other problems (see Experimental Procedures).

Formulation and Structure. Having established the existence of a homogeneity range for Zr_5Sb_3-M as approximately $Zr_5Sb_{3.0}$ to $Zr_5Sb_{3.4}$, the question of formulation now arises. Although the composition may be represented by the zirconium-deficient $Zr_{5-z}Sb_3$ as readily as by the antimony-rich Zr_5Sb_{3+x}, there are compelling reasons for the latter. The stoichiometric Zr_5Sb_3 in the Mn_5Si_3 structure contains an empty site in the center of a relatively large zirconium trigonal antiprism around the origin of the unit cell (see below). In many other cases,[3-5] an impurity atom is found or is thought to occur at this site and to thereby stabilize the structure, and this was also suspected for Zr_5Sb_3-M. However, the impurity explanation can be eliminated by the reproducible, 100% yields of Zr_5Sb_3-M obtained in many different reactions. Furthermore, as illustrated above, the lattice parameters of this phase demonstrate a linear dependence on antimony content over a significant range in the antimony-rich region. Actually, the conclusion that this must represent a nonstoichiometric binary phase can be fully appreciated only in the light of experimental results obtained with many possible impurity elements.[3] For example, the stipulation that the phase is essentially oxygen-free is buttressed by results obtained when oxygen is intentionally added to the system. Sintering of suitable amounts of powdered Zr, Sb, and ZrO_2 produces a Mn_5Si_3-type phase with much smaller lattice parameters: a = 8.3146 (6) Å, c = 5.6954 (4) Å (compare Table III, reactions 4 and 5).

The occupation of the interstitial site by antimony also seems more likely than the occurrence of zirconium vacancies on the basis of the examples of Ti_5Ga_4[15] and Zr_5Sn_4,[16] which have "filled" Mn_5Si_3 structures in which the fourth main-group atom is bound in the so-called interstitial site, viz., $(Ti_5Ga_3)Ga$ and $(Zr_5Sn_3)Sn$. This circumstance was confirmed by a single-crystal structural investigation of a particular Zr_5Sb_{3+x}-M composition, the results for which are given in Table V. The refined partial occupancy of only this site yields an overall composition of $Zr_5Sb_{3.161(7)}$. This result compares well with the compositions calculated from the previously derived linear least-squares fit to powder pattern lattice constants (Figure 3). The latter yield, for each lattice constant, x_a = 3.14 and x_c = 3.13 for this sample, slightly smaller than the single-crystal result, 3.16, but not seriously so, consistent with a possible small systematic error in the powder data (see above). In any case, the dimensions obtained for the single crystal are quite compatible with those of known homogeneous Zr_5Sb_{3+x} samples.

A projection of the Zr_5Sb_3-M structure down the hexagonal c axis is drawn in Figure 4. All atoms are located in special positions; those with fixed z parameters $^1/_4$ and $^3/_4$ are represented by the corresponding shading of the atoms, while filled circles depict atoms at z = 0 *and* $^1/_2$. The structure can be described in terms of two types of chains that extend along the c axis, as

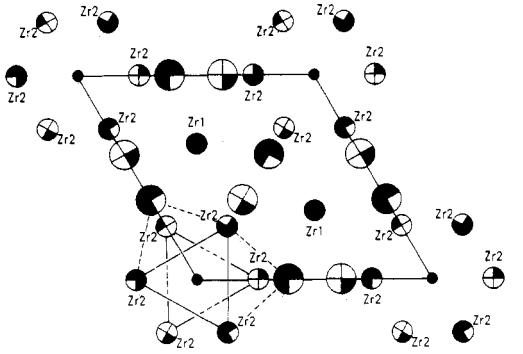

Figure 4. Projection of the Zr_5Sb_3-M structure (Mn_5Si_3 type) onto (001), with arbitrary thermal ellipsoid sizes. Large circles are antimony atoms, medium circles are zirconium atoms, and small circles mark the interstitial sites at the unit cell origin. Fractional shading of each atom represents its height along the c axis. The filled circles occur at both z = 0 and z = $^1/_2$. The solid lines outline the zirconium trigonal antiprism, and the dashed lines, two of the edge-bridging antimony atoms.

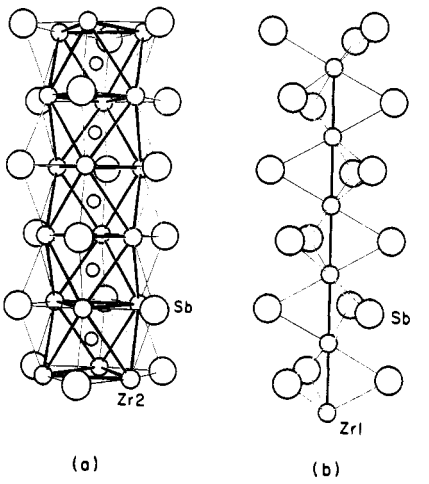

Figure 5. Separate views of (a) the condensed octahedral Zr(2) chain and (b) the linear Zr(1) chain in Zr_5Sb_3-M (Mn_5Si_3-type structure). Large circles denote antimony atoms, medium circles denote zirconium atoms, and small circles denote interstitial Z. Note that Zr(1) and the interstitial site occur at the same height along c and have the same interatomic spacing.

shown in Figure 5. The Zr(1) atoms define a linear chain (Figure 5b) with an extremely short Zr–Zr interatomic distance of $c/2$ = 2.893 (1) Å compared with 3.20-Å separations in hcp α-Zr and 2.92 Å for the single-bond length.[17] This chain of very closely spaced transition metals is a notable feature of the Mn_5Si_3 structure type and is reminiscent of similar chains of transition metals (T) in many T_3B compounds that have the A-15 structure. A significant difference in the Mn_5Si_3 structure is that the chains extend only in one direction, not the three found in the cubic A-15's. The Zr(1) atoms in these chains are coordinated by six Sb(1) atoms at a distance of 2.974 (1) Å in this particular phase, typical of Zr–Sb spacings in other binary compounds.[2] The surrounding polyhedron is somewhat unusual in that the coordination cannot be described as trigonal prismatic or trigonal antiprismatic but intermediate between the two extremes.

The second and chemically more significant structural feature is that formed by the Zr(2) atoms. This can be viewed as an infinite stack of confacial octahedra, more properly trigonal antiprisms, as illustrated in Figure 5a. The interesting interstitial site at 0, 0, 0 is centered in these polyhedra. In contrast to the separations in the Zr(1) chain, the Zr(2)–Zr(2) interatomic distances are very long, 3.56 and 3.60 Å, and in fact, the interchain Zr(1)–Zr(2) distance at 3.55 Å is comparable. The Sb(1) atoms can be viewed as capping edge-sharing pairs of exposed triangular

(15) Pötzschke, M.; Schubert, K. *Z. Metallkd.* **1962**, *53*, 474.
(16) Schubert, K.; Meissner, H. G.; Raman, A.; Rossteutscher, W. *Naturwissenschaften* **1964**, *54*, 284.
(17) Corbett, J. D. *J. Solid State Chem.* **1981**, *37*, 335.

faces on the confacial zirconium octahedral chain or, alternatively, as bridging those shared edges (Figure 4). The resulting isolated chain can be formulated $^1_\infty[Zr_{6/2}Sb_{6/2}]$, although it should be noted that each antimony therein is also strongly bonded to both a Zr(2) vertex in another Zr_3Sb_3 chain, a common behavior, and to four members of the Zr(1) chains described earlier. These bonds serve to make the structure a good deal less anisotropic than is implied by Figure 5 alone.

A nominally ideal solid solution behavior of antimony in this interstitial site in Zr_5Sb_3 is manifested in the evidently linear increase of lattice parameters with increasing antimony content (Vegard's law) (Figure 3). Stability in this system does not extend to $x = 1$ (Zr_5Sb_4) as it does in Zr_5Sn_4.[3]

Many of the same structural features of the lower limit Zr_5Sb_3 are found in the condensed M_6X_8 cluster compound KMo_3S_3.[18] The two structures are actually very similar, but a major difference comes about when each potassium is replaced by a pair of Zr(1) atoms in the linear metal chain.

The possibility that some Zr_5Sb_{3+x} compositions may exhibit an ordered interstitial distribution (superstructure) was also considered. Superstructures based on the Mn_5Si_3 structure have been observed in the powder patterns of rare-earth-metal silicides in which carbon has been added as a ternary component and presumably occupies the interstitial site.[19-21] Unlike the situation for Zr_5Sb_{3-x}-M, x in $R_5Si_3C_x$ (R = Gd, Ho, Er) can evidently be varied from 0.0 to 1.0, and a $\sqrt{3}a$ superstructure was observed at $x \simeq 0.5$ for all three metals, plus an additional tripling of the c axis at $x = 1.0$ for Er and Ho. ($x > 0.75$ is not in accord with simple valence rules, however, and a $\sqrt{3}a$ superstructure alone can arise from the Ca_5Pb_3-type alternative.[3]) The plot of lattice parameters versus composition for $Gd_5Si_3C_x$ varied markedly from linearity.[21] Despite the obvious differences between Zr_5Sb_{3+x} and $R_5Si_3C_x$ systems, the possibility of superstructure formation in the former was investigated.

The Guinier powder patterns of 23 reactions that yielded single-phase Zr_5Sb_3-M product were carefully examined, and 17 were found to exhibit no evidence of additional superstructure lines. These samples had been prepared by a variety of techniques and included arc-melted, both as-cast and annealed (T = 1000–1100 °C), products as well as sintered powders (T = 1000–1100 °C) with and without an added transport agent. The remaining six reactions did exhibit weak diffraction lines indicative of a superstructure.

All of these six reactions were from a series designed to produce additional lattice parameter vs composition data. They utilized ground mixtures of $Zr_5Sb_{3.0}$ prepared by arc melting and antimony that had been sealed in Ta containers and heated in a vacuum furnace ($\sim 10^{-5}$ Torr) at 1300 °C for 3 days. A series of six Zr_5Sb_{3+x} compounds ($0.15 \leq x \leq 0.50$) was supposed to have been produced by these reactions, but the lattice parameters for all of the 5:3 products were virtually identical and were within experimental error the same as the values for the antimony-rich limit $Zr_5Sb_{3.4}$ (Figure 3). This was so because some ZrO_2 had also been formed in the reactions, presumably because of an inadequate vacuum, and this effectively decreased the Zr:Sb ratio. The two reactions originally loaded for the largest values of x also contained the strongest lines of $ZrSb_{1-x}$[2] in their powder patterns (two lines and one line, respectively). Other reactions may also have contained this phase below the detection limit of Guinier powder diffraction ($\sim 3\%$). More to the point, most of the powder patterns of this upper limit Zr_5Sb_{3+x} also exhibited the same three or four very weak extra lines, and these could be indexed on a larger hexagonal cell with $a = \sqrt{3}a$, the same effect observed with $R_5Si_3C_{0.5}$. But the simultaneous presence of ZrO_2 in all products,

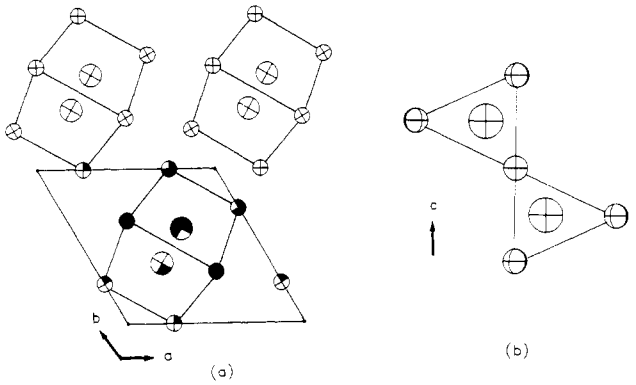

Figure 6. (a) Side view of the chain of trigonal prisms of zirconium in Zr_5Sb_3-M (Mn_5Si_3). Larger circles are antimony atoms; smaller circles are zirconium atoms. In the interest of clarity only the atoms in the trigonal prism chain are drawn. Fraction shadings of the atoms represent their heights along the c axis; filled circles occur at both $z = 0$ and $z = 1/2$. (b) Clearer view of the antimony-centered trigonal prisms along $\vec{c}$. Note that these alternately face in opposite directions.

and *only* in this particular reaction set, makes any conclusion tenuous.

There is a clear temperature dependence for the formation of $Zr_5Sb_{3.0}$-M vs Zr_5Sb_3-Y. The latter in the Y_5Bi_3 structure is isolated only as a metastable phase from high-temperature preparations. The lattice constants of Zr_5Sb_3-M that accompanies Zr_5Sb_3-Y in as-cast preparations for $x < \sim 0.2$ are essentially the same as those measured for $Zr_5Sb_{3.16(7)}$, meaning that a small amount of (undetected) Zr_3Sb should also be present. The behavior implies that the transformation between the Y_5Bi_3 structure and the Mn_5Si_3 modification at high temperatures is an incongruent process. There is also a compositional dependence since Zr_5Sb_3-Y has an extremely narrow homogeneity range and Zr_5Sb_3-M has an extensive one. Any excess of antimony will thus favor the formation of the latter structure.

Comparisons. The same pairs of structural modifications have been observed for R_5Bi_3 phases as well, namely, for Gd_5Bi_3 and Tb_5Bi_3.[22] The Y_5Bi_3-type structure was also obtained from melted alloys with the more lanthanide rich compositions. The authors accordingly initially formulated the phases as R_5Bi_3 for the Mn_5Si_3-type structure and $R_{5+x}Bi_3$ for the Y_5Bi_3 modification. A subsequent crystal structure refinement of Y_5Bi_3 established that it was stoichiometric with no excess rare-earth metal, and so the Mn_5Si_3 polymorph was then described as $R_{5-x}Bi_3$.[13] The results of the present investigation of Zr_5Sb_3 strongly imply that the Mn_5Si_3 modifications of Gd_5Bi_3 and Tb_5Bi_3 should be rewritten once again, now as R_5Bi_{3+x}.

The structural relationship between the Y_5Bi_3 and Mn_5Si_3 types described for the R_5Bi_3 phases[13] is equally applicable to the two Zr_5Sb_3 compounds. A structural feature that is common to both structure types can be discerned. As seen in Figure 1, zigzag chains of opposite-facing and edge-sharing zirconium trigonal prisms centered by antimony atoms lie along the [101] plane in Zr_5Sb_3-Y. Other atoms in the structure form a network of diamonds and pentagons (not shown). Similar chains of opposite-facing zirconium trigonal prisms sharing long edges can also be found in Zr_5Sb_3-M along the [001] direction, as illustrated in Figure 6, but these chains are now linear and not buckled as in Zr_5Sb_3-Y. Here, the network of zirconium and antimony atoms around the prisms forms a ribbon of triangles sharing edges (not shown). The distortion of Zr_5Sb_3-M to form Zr_5Sb_3-Y results from the buckling of these prism chains and also causes the regular network of triangles to form the pentagons and diamonds noted above.

However, the differences between the two structures cannot be ascribed solely to a simple distortion of the prism chains. In Zr_5Sb_3-Y the prisms also share opposed trigonal faces to form

(18) Potel, M.; Chevrel, R.; Sergent, M.; Decroux, M.; Fischer, Ø. *C. R. Seances Acad. Sci., Ser. C* **1979**, *288*, 429.
(19) Al-Shahery, G. Y. M.; Jones, D. W.; McColm, I. J.; Steadman, R. *J. Less-Common Met.* **1982**, *85*, 233.
(20) Al-Shahery, G. Y. M.; Jones, D. W.; McColm, I. J.; Steadman, R. *J. Less-Common Met.* **1983**, *87*, 99.
(21) Al-Shahery, G. Y. M.; Steadman, R.; McColm, I. J. *J. Less-Common Met.* **1983**, *92*, 329.
(22) Yoshihard, K.; Taylor, J. B.; Calvert, L. D.; Despault, J. G. *J. Less-Common Met.* **1975**, *41*, 329.

sheets composed of trigonal columns about (101). These planes are connected by sharing the remaining edges to constitute the three-dimensional structure and to give the large hexagonal channels (Figure 1). The connectivity of the trigonal prisms in Zr_5Sb_3-M is very different. The prisms do not share either the trigonal faces or the remaining third edge (Figure 6). Thus, a considerable rearrangement is required to convert the Y_5Bi_3-type into the Mn_5Si_3-type structure. This is likely not a concerted process, which could account for some of the apparently large kinetic barriers found for their interconversion.

The interstitial site at the center of the zirconium octahedra in Zr_5Sb_3-M has a counterpart in Zr_5Sb_3-Y; it is, however, a tetrahedral site with a distance of ~2.1 Å from the neighboring zirconium atoms. This position is much too small to accommodate any excess antimony without a very large distortion. Extra antimony atoms can be bonded much more easily in the interstitial site of Zr_5Sb_3-M and are likely to be the cause of the adoption of the Mn_5Si_3 structure for Zr_5Sb_{3+x} compositions. A small nonmetal (B, C, N) atom would be more likely physically to fit in the former tetrahedral site. However, investigations of these Zr_5Sb_3Z systems have shown that even such small nonmetal atoms prefer the octahedral hole in the Mn_5Si_3 modification, although tetrahedral site occupancy has been found in other examples of the Yb_5Sb_3 structure type.[3] Details will be forthcoming.

Acknowledgment. The crystallographic and computing facilities were graciously provided by R. A. Jacobson, while arc-melting equipment was kindly made available to us by H. F. Franzen.

Supplementary Material Available: Table of anisotropic thermal parameters for Zr_5Sb_3-Y and Zr_5Sb_3-M (1 page); listings of observed and calculated structure factors for the same compounds (3 pages). Ordering information is given on any current masthead page.

Contribution from the Department of Chemistry,
University of Tennessee, Knoxville, Tennessee 37996-1600

Raman Spectroscopy of Fluoride-Containing Chloroaluminate Melts

B. Gilbert,† Stephen D. Williams,‡ and G. Mamantov*

Received December 23, 1987

The effect of adding fluoride ions to chloroaluminate melts has been studied by Raman spectroscopy. In acidic (AlX_3/MX mole ratio greater than 1, where M^+ is an alkali-metal ion) melts at 200 °C, the fluoride ion acts as a dibase and the new species $Al_2Cl_6F^-$ is formed, as indicated by comparison of observed and calculated frequencies. The polarization of the Raman bands indicates that a fluoride replaces a terminal chloride. Measurements have also been made on several basic melts (AlX_3/MX mole ratio <1) at much higher temperatures (between 580 and 850 °C). The best results were obtained at 820 °C for mixtures of $NaAlCl_4$ with increasing amounts of NaF. It was found that fluoride replaces chloride progressively, depending on the molar ratio of NaF to $NaAlCl_4$. The new species $AlCl_3F^-$, $AlCl_2F_2^-$, and $AlClF_3^-$, together with the previously observed AlF_4^-, are clearly identified. Intensity measurements made on the characteristic bands allow a quantitative study of the distribution of each species as a function of melt composition. The calculated equilibrium constants follow the same trend as was found for similar chloro bromo species.

Introduction

Aluminum halide containing molten salt systems are of major importance to aluminum production; they are also of interest for high-energy batteries. Unusual redox and coordination chemistry has been observed in these melts.[1,2] The haloaluminate ions present in these melts are usually formed by the reaction between the alkali-metal halide and an aluminum halide, although lower melting point systems formed with organic halides have also been studied.[3] Mixed-halide melts have received some attention: for example, chlorobromoaluminate and chloroiodoaluminate systems have been studied by spectroscopic methods,[4-7] while electrochemical methods have been used to probe the behavior of F^- ion in acidic chloroaluminate melts.[8]

Tetrachloroaluminate ion has been shown to undergo fast exchange with a higher mass halogen (Br, I), in the liquid state (in CH_3CN solutions or in the molten state).[4-7] Vibrational spectroscopy and ^{27}Al NMR measurements provide evidence that when $AlCl_4^-$ is mixed with $AlBr_4^-$ or AlI_4^- the various mixed ions $AlCl_nX_{4-n}^-$ (X = Br, I) are formed, with n depending only on the mole ratio of the respective halides.[4-7]

Mixtures of $AlCl_4^-$ and fluoride ion should also exhibit similar behavior; however, no spectroscopic studies of such species have been reported, except for the Raman spectroscopic characterization of simple fluoro complexes, AlF_4^- and AlF_6^{3-}, in fluoride melts.[9,10]

In this paper we describe Raman spectroscopic studies of several new species formed by the exchange of fluoride for chloride in chloroaluminate melts.

Experimental Section

All chemicals were purified by the usual methods for chloroaluminate melt preparation.[11,12] The alkali-metal chlorides were melted in quartz tubes, treated with HCl and nitrogen, and crystallized from the melt. $AlCl_3$ (from Fluka) was distilled twice. NaF was melted in a nickel crucible and recrystallized twice by slow cooling. Clear crystals of each starting material were used to make the mixtures. Chemicals were handled in a drybox (water level <1 ppm) or under vacuum.

Because of the much lower viscosity of the present melts compared to that of pure fluoride melts, a windowless cell such as that used previously[13] was found to be impractical. With the size of the main holes

†Permanent address: Department of Chemistry, University of Liege, Liege, Belgium.
‡Permanent address: Department of Chemistry, Appalachian State University, Boone, NC 28608.

(1) Mamantov, G.; Osteryoung, R. A. In *Characterization of Solutes in Non-Aqueous Solvents*; Mamantov, G., Ed.; Plenum: New York, 1978; pp 223-249.
(2) Boston, C. R. In *Advances in Molten Salt Chemistry*; Braunstein, J., Mamantov, G., Smith, G. P.; Eds.; Plenum: New York, 1971; Vol. 1, pp 129-163.
(3) Hussey, C. L. In *Advances in Molten Salt Chemistry*; Mamantov, G., Ed.; Elsevier: New York, 1983; Vol. 5, pp 185-230.
(4) Bradley, B. H.; Brier, N. P.; Jones, D. E. H. *J. Chem. Soc. A* **1971**, 1397.
(5) Jones, D. E. H. *J. Chem. Soc., Dalton Trans.* **1972**, 567.
(6) Berg, R. W.; Kemnitz, E.; Hjuler, H. A.; Fehrmann, R.; Bjerrum, N. J. *Polyhedron* **1985**, *4*, 457.
(7) Kidd, R. G.; Truax, D. R. *J. Am. Chem. Soc.* **1968**, *90*, 6867.
(8) Tremillon, B.; Duchange, J. P. *J. Electroanal. Chem. Interfacial Electrochem.* **1973**, *44*, 389.
(9) Gilbert, B.; Mamantov, G.; Begun, G. M. *Inorg. Nucl. Chem. Lett.* **1974**, *10*, 1123.
(10) Gilbert, B.; Mamantov, G.; Begun, G. M. *J. Chem. Phys.* **1975**, *62*, 950.
(11) Torsi, G.; Fung, K. W.; Begun, G. M.; Mamantov, G. *Inorg. Chem.* **1971**, *10*, 2285.
(12) Marassi, R.; Chambers, J. Q.; Mamantov, G. *J. Electroanal. Chem. Interfacial Electrochem.* **1976**, *69*, 345.
(13) Gilbert, B.; Mamantov, G.; Begun, G. M. *Appl. Spectrosc.* **1975**, *29*, 276.

0020-1669/88/1327-2359$01.50/0